

Competing Exchange Interactions in the Multiferroic and Ferrimagnetic $\text{CaBaCo}_4\text{O}_7$ ^{*}

R.S. Fishman¹, S. Bordács², V. Kocsis², I. Kézsmárki², J. Viirok³, U. Nagel³, T. Rőõm³, A. Puri⁴, U. Zeitler⁴, Y. Tokunaga^{5,6}, Y. Taguchi⁵, and Y. Tokura^{5,7}

¹Materials Science and Technology Division, Oak Ridge National Laboratory, Oak Ridge, Tennessee 37831, USA

²Department of Physics, Budapest University of Technology and Economics and MTA-BME

Lendület Magneto-optical Spectroscopy Research Group, 1111 Budapest, Hungary

³National Institute of Chemical Physics and Biophysics, Akadeemia tee 23, 12618 Tallinn, Estonia

⁴High Field Magnet Laboratory (HFML-EMFL), Radboud University Nijmegen,

Toernooiveld 7, 6525 ED Nijmegen, The Netherlands

⁵RIKEN Center for Emergent Matter Science (CEMS), Wako, Saitama 351-0198, Japan

⁶Department of Advanced Materials Science, University of Tokyo, Kashiwa 277-8561, Japan and

⁷Department of Applied Physics, University of Tokyo, Hongo, Tokyo 113-8656, Japan

(Dated: June 8, 2019)

Competing exchange interactions can produce complex magnetic states associated with spin-induced electric polarizations. With competing interactions on alternating triangular and kagome layers, $\text{CaBaCo}_4\text{O}_7$ may have one of the largest measured spin-induced polarizations of ~ 1700 nC/cm² below its ferrimagnetic transition temperature at 70 K. Powder neutron-diffraction data, magnetization measurements, and spin-wave resonance frequencies in the THz range reveal that the complex spin order of multiferroic $\text{CaBaCo}_4\text{O}_7$ can be described as a triangular array of *c*-axis chains ferromagnetically coupled to each other in the *ab* plane. Magnetostriction for a set of spin bonds within each chain produces the large spin-induced polarization of $\text{CaBaCo}_4\text{O}_7$.

PACS numbers: 75.25.-j, 75.30.Ds, 75.50.Ee, 78.30.-j

Competing exchange interactions produce complex magnetic states with a wide range of interesting behavior found in spin glass [1], spin ice [2], and magnetic skyrmions [3]. In multiferroic materials, complex spin states can exhibit a spin-induced electric polarization \mathbf{P} due to either the spin current, *p-d* orbital hybridization, or magnetostriction [4,5]. Because the coupling between the electrical and magnetic properties in multiferroic materials is both scientifically and technologically important, the effects of competing exchange interactions have been investigated in a wide range of multiferroic materials such as $RMn\text{O}_3$ [6], CoCrO_4 [7], CuCrO_2 [8], CuFeO_2 [9], and MnWO_4 [10]. While the first four materials [6–9] are geometrically frustrated due to competing interactions on a triangular lattice, MnWO_4 [10] exhibits long-range competing interactions [11] on a highly-distorted monoclinic lattice.

Compounds in the “114” family [12–14] $RBa\text{Co}_4\text{O}_7$ contain alternating triangular and kagome layers, both of which are geometrically frustrated in the absence of any distortions. This family was initially studied to find

charge ordering among the Co^{2+} and Co^{3+} ions. An important member of this family, YBaCo_4O_7 exhibits antiferromagnetic ordering [15,16] below 110 K and diffuse scattering [12,13] indicative of spin disorder below 60 K. The magnetic state between 110 K and 60 K is stabilized by a structural transition [17] that relieves the geometric frustration and confines the spins to the *ab* plane. Both the structural and magnetic transitions are quite sensitive to excess oxygen and no magnetic order [18,19] is found in $\text{YBaCo}_{4\delta}\text{O}_{7+\delta}$ for $\delta \geq 0.12$. Another family member, $\text{YbBaCo}_4\text{O}_7$ undergoes a structural transition at 175 K that relieves the geometric frustration and stabilizes an antiferromagnetic state below 80 K [20].

A particularly interesting member of the “114” family, $\text{CaBaCo}_4\text{O}_7$ was recently [21] found to have a very large spin-induced polarization ~ 1700 nC/cm², second only to the conjectured [22] spin-induced polarization ~ 3000 nC/cm² of BiFeO_3 . Also usual, this multiferroic compound develops a substantial ferrimagnetic moment [23] of about 0.9 μ_B per formula unit (f.u.) below $T_c = 70$ K. In principle, this could allow magnetic control of the ferroelectric polarization. Because its ferroelectric transition is inaccessible and its permanent electric polarization is so large, $\text{CaBaCo}_4\text{O}_7$ is properly classified as a pyroelectric [24] with a non-switchable electric polarization.

In this Letter, we solve for the magnetic properties of $\text{CaBaCo}_4\text{O}_7$ based on a Heisenberg model with 12 nearest neighbor interactions and associated anisotropies. This model reveals that $\text{CaBaCo}_4\text{O}_7$ finds a novel way to reduce magnetic frustration on a spin state that can be described as a triangular array of ferromagnetically aligned *c*-axis chains. Competing interactions within each chain produce a non-collinear spin state that supports a strong

^{*}Copyright notice: This manuscript has been authored by UT-Battelle, LLC under Contract No. DE-AC05-00OR22725 with the U.S. Department of Energy. The United States Government retains and the publisher, by accepting the article for publication, acknowledges that the United States Government retains a non-exclusive, paid-up, irrevocable, world-wide license to publish or reproduce the published form of this manuscript, or allow others to do so, for United States Government purposes. The Department of Energy will provide public access to these results of federally sponsored research in accordance with the DOE Public Access Plan (<http://energy.gov/downloads/doe-public-access-plan>).

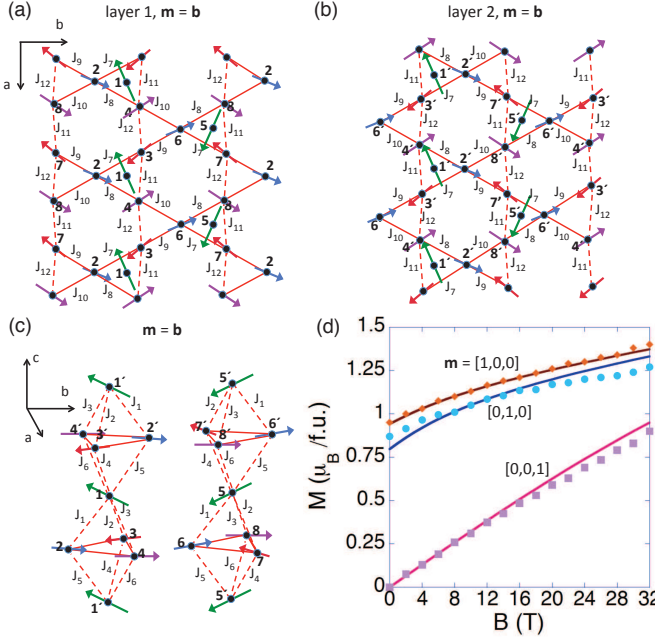


FIG. 1: (Color online) (a) and (b) The predicted spin configuration for layers 1 and 2 with field orientation $\mathbf{m} = \mathbf{b}$. (c) A sideways view of this configuration. (d) The measured (circles and squares) and predicted (solid curves) magnetizations for field along $[1, 0, 0]$, $[0, 1, 0]$, or $[0, 0, 1]$.

strong spin-induced electric polarization below T_c due to the electric-field dependence of those interactions, called magnetostriction.

As shown in Fig. 1, Co atoms form a connected tetrahedral network with alternating kagome and triangular layers. An orthorhombic distortion [25] above T_c relieves the geometric magnetic frustration on both the distorted kagome and triangular layers. Below T_c , the distorted structure stabilizes a complex ferrimagnetic state with net moment along \mathbf{b} .

Each magnetic unit cell of $\text{CaBaCo}_4\text{O}_7$ contains 16 Co ions on two kagome and two triangular layers with orthorhombic lattice constants $a = 6.3 \text{ \AA}$, $b = 11.0 \text{ \AA}$, and $c = 10.2 \text{ \AA}$. Four crystallographically distinct Co ions have three different valences [25,26]. The triangular layers contain mixed-valent $\text{Co}^{3+}/\text{Co}^{2+}\underline{L}$ spins 1, 5, 9, and 13 with moments $M_1 = 2.9 \mu_B$. The kagome layers contain Co^{2+} spins 2, 3, 6, 7, 10, 11, 14, and 15 with moments $M_2 = M_3 = 2 \mu_B$ and mixed-valent $\text{Co}^{3+}/\text{Co}^{2+}\underline{L}$ spins 4, 8, 12, and 16 with $M_4 = 2.4 \mu_B$. Because adjacent kagome or triangular layers are related by symmetry, $\mathbf{S}_{i'} = \mathbf{S}_{i+8}$ on layer two is identical to \mathbf{S}_i on layer one. With $\mathbf{S}_i = S_i(\cos \phi_i, \sin \phi_i, 0)$ constrained to the ab plane, the ferrimagnetic moment lies along \mathbf{b} if $\phi_{i+4} = \pi - \phi_i$ ($i = 1, \dots, 4$).

The 12 different nearest-neighbor exchange couplings J_i are drawn in Figs. 1(a-c). Six of these (J_1 through J_6) couple the kagome and triangular layers as shown in Fig. 1(c); the other six (J_7 through J_{12}) couple the spins within a kagome layer as shown in Figs. 1(a) and

(b). To guarantee that the the spin configuration repeats on next-neighbor layers ($\mathbf{S}_{i'} = \mathbf{S}_i$), we assume that $J_5 = J_1$, $J_4 = J_2$, and $J_6 = J_3$, although these equalities are not required by symmetry. The dominance of nearest-neighbor exchange over next-nearest neighbor exchange [24] justifies setting the exchange interactions between spins on the triangular layers to zero. Our model also includes easy-plane anisotropies D and easy-axis anisotropies C within both kagome and triangular layers. Hexagonal anisotropy A is included on the triangular layers.

With magnetic field \mathbf{B} along \mathbf{m} , the Hamiltonian is

$$\begin{aligned} \mathcal{H} = & - \sum_{\langle i,j \rangle} J_{ij} \mathbf{S}_i \cdot \mathbf{S}_j + D^{\text{tri}} \sum_{i,\text{tri}} S_{ic}^2 + D^{\text{kag}} \sum_{i,\text{kag}} S_{ic}^2 \\ & - C^{\text{kag}} \sum_{i,\text{kag}} (\mathbf{o}_i \cdot \mathbf{S}_i)^2 - C^{\text{tri}} \sum_{i,\text{tri}} (\mathbf{n}_i \cdot \mathbf{S}_i)^2 \\ & - A^{\text{tri}} \sum_{i,\text{tri}} \left\{ (S_{ia} + iS_{ib})^6 + (S_{ia} - iS_{ib})^6 \right\} \\ & - 2\mu_B B \sum_i \mathbf{m} \cdot \mathbf{S}_i, \end{aligned} \quad (1)$$

where the easy-axis anisotropy terms proportional to C^{kag} and C^{tri} involve unit vectors \mathbf{o}_i along the “bowtie” directions $\phi_i = \pi/2$ (spins 2 and 6), $5\pi/6$ (spins 3 and 8) and $7\pi/6$ (spins 4 and 7) for the kagome layers and \mathbf{n}_i along the $\phi_i = \pi/6$ (spin 1) and $-\pi/6$ (spin 5) directions for the triangular layers. In equilibrium, the hexagonal anisotropy term proportional to A^{tri} reduces to $-2A^{\text{tri}} S_1^6 \cos 6\phi_i$ (spins 1 and 5) on the triangular layers. Note that all anisotropy terms may constrain the spins to the ab plane.

Static properties of this model are obtained by minimizing the classical energy $\langle \mathcal{H} \rangle$ with respect to the 16 spin angles. Dynamical properties are obtained from a $1/S$ expansion about the classical limit. The eigenvalues and eigenvectors of the 32×32 equations-of-motion matrix [27] give the optical mode frequencies and their absorptions, respectively.

Perhaps due to excess or deficient oxygen [28] or different domain populations (see below), previous magnetization measurements [23,25,29–31] on $\text{CaBaCo}_4\text{O}_7$ are rather scattered. Our fits are based on new magnetization measurements performed on twinned crystals with a common $\mathbf{c} = \mathbf{z} = [0, 0, 1]$ axis. As shown below from the periodicity of the spin-wave mode frequencies as the field is rotated about \mathbf{z} , our crystals are hexagonally twinned. In domain I, \mathbf{a} lies along the laboratory direction $\mathbf{x} = [1, 0, 0]$ and \mathbf{b} lies along $\mathbf{y} = [0, 1, 0]$; in domain II, $\mathbf{a} = [-1/2, \sqrt{3}/2, 0]$ and $\mathbf{b} = [-\sqrt{3}/2, -1/2, 0]$; and in domain III, $\mathbf{a} = [-1/2, -\sqrt{3}/2, 0]$ and $\mathbf{b} = [\sqrt{3}/2, -1/2, 0]$. If p_n are the domain populations, then the magnetizations M_x and M_y measured with fields along \mathbf{x} and \mathbf{y} only depend on p_1 and $p_2 + p_3 = 1 - p_1$. Of course, M_z measured with field along \mathbf{z} is independent of p_n . Measurements in Fig. 1(d) indicate that all three magnetizations increase monotonically up to at least 32 T.

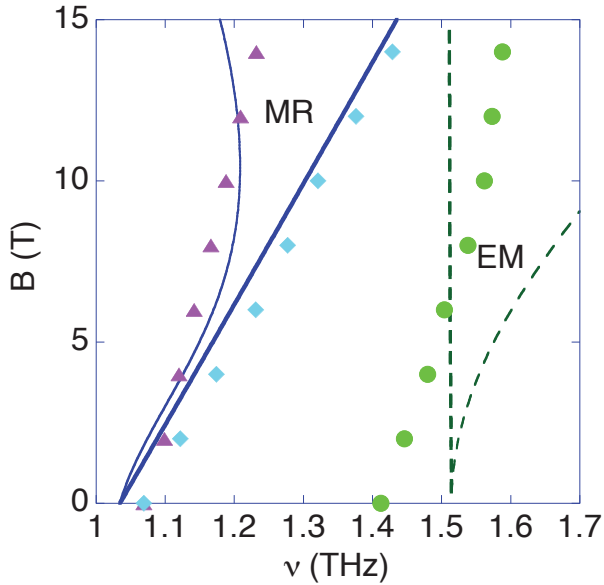


FIG. 2: (Color online) The predicted MR (solid) and EM (dashed) modes for domain I (thick) and domains II and III (thin). Measured modes are indicated by solid points.

Previous optical measurements [32] revealed two conventional spin-wave modes that couple to the ground state through the magnetization operator $\mathbf{M} = 2\mu_B \sum_i \mathbf{S}_i$. These magnetic-resonance (MR) modes are degenerate in zero field with a frequency of 1.07 THz and split almost linearly with increasing field along \mathbf{y} , as shown in Fig. 2. For $\mathbf{m} = \mathbf{y}$, the MR modes are excited in two geometries: (i) with THz fields $\mathbf{E}_\omega \parallel \mathbf{x}$ and $\mathbf{B}_\omega \parallel \mathbf{z}$ and (ii) with $\mathbf{E}_\omega \parallel \mathbf{z}$ and $\mathbf{B}_\omega \parallel \mathbf{x}$. CaBaCo₄O₇ also supports an electromagnon (EM) that couples to the ground state through the polarization operator \mathbf{P} . The EM with zero-field frequency 1.41 THz in Fig. 2 is only excited in geometry *ii*.

Because the exchange couplings already break every degeneracy in the unit cell, the 16 predicted modes for a single domain are non-degenerate. Therefore, the split MR modes must come from different domains. We verified this by measuring [33] the MR mode frequencies as a function of the rotation angle θ for field $\mathbf{B} = B(\cos \theta, \sin \theta, 0) = B(\mathbf{x} \cos \theta + \mathbf{y} \sin \theta)$ in the laboratory reference frame. As shown in Fig. 3 for 12 and 15 T, the three MR mode frequencies have an overall periodicity of $\pi/3$. Each hexagonal domain contributes one branch of excitations with a period of π .

With field $\mathbf{B}_{loc} = B(\cos \psi, \sin \psi, 0) = B(\mathbf{a} \cos \psi + \mathbf{b} \sin \psi)$ in the local reference frame of a given domain, the upper MR mode in Fig. 2 corresponds to the $\psi = \pi/2$ mode for domain I while the lower MR mode corresponds to the degenerate $\psi = \pm\pi/6$ modes for domains II and III. The previously measured MR mode frequencies plotted in Fig. 2 at 12 T correspond to the diamond and triangular points in Fig. 3(b) at $\theta = \pi/2$. Cusps in the MR curves for each domain at $\psi = 0$ and π are caused

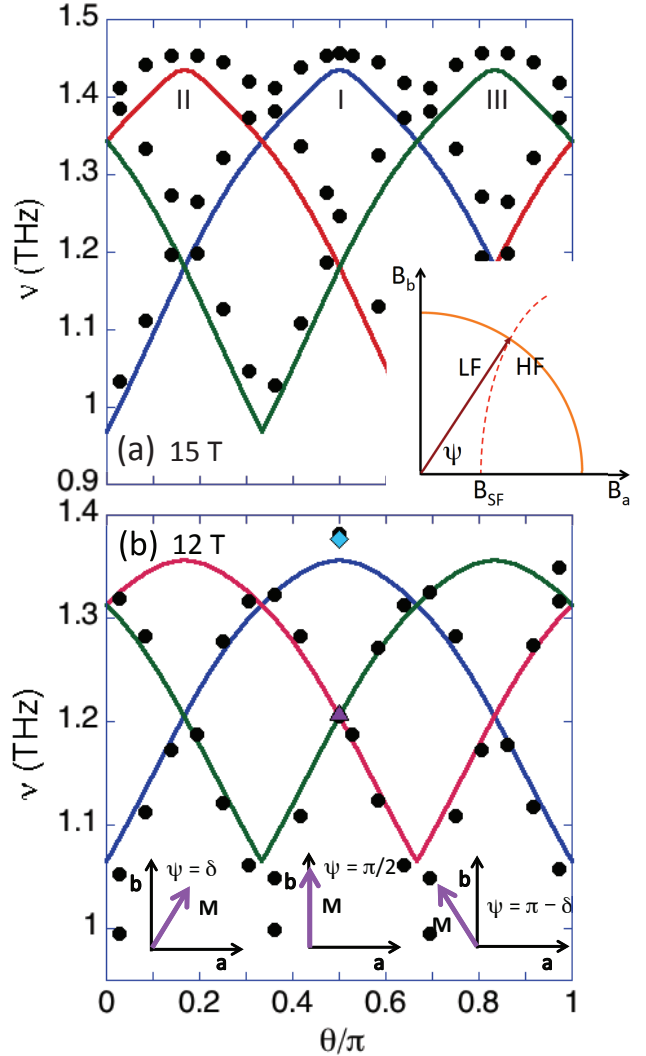


FIG. 3: (Color online) The measured (solid circles) and predicted (blue, red, and green curves for domains I, II, and III, respectively) angular dependence of the MR mode frequencies for 12 and 15 T. The inset to (a) sketches the angular dependence of \mathbf{B}_{SF} (dashed curve), which separates low-field (LF) and high-field (HF) states. A jump in the mode frequencies is expected when the local field $\mathbf{B}_{loc}(\psi)$ for any domain crosses that boundary. The inset to (b) shows the net magnetization of any domain for three angles ψ . Flips of the b -axis spin at $\psi = 0$ and π produce the cusps in the mode frequencies.

by flipping the b component of the magnetization. Just above $\psi = 0$ or just below π , \mathbf{M} has a significant component along \mathbf{b} ; just below $\psi = 0$ or just above π , \mathbf{M} has a significant component along $-\mathbf{b}$ (see inset to Fig. 3(b)).

Fits for the coupling parameters utilize the field dependence of \mathbf{M} , the zero-field powder neutron-diffraction data [25], the field dependence of the MR and EM modes at $\theta = \pi/2$ [32], and the MR mode frequencies at $\theta = 0$ and $\pi/3$ for 7, 12 and 15 T. The resulting exchange and anisotropy constants are provided in Table I and the corresponding zero-field spin state is plotted in Figs. 1(a-c).

TABLE I: Exchange and anisotropy parameters in meV.

p_1	$J_1 = J_5$	$J_2 = J_4$	$J_3 = J_6$	J_7	J_8	J_9	J_{10}	$J_{11} = J_{12}$	D^{kag}	D^{tri}	C^{kag}	C^{tri}	$S_1 A^{\text{tri}}$	
0.19	-95.3	-10.1	43.9	-26.5	183	4.5	30.6	-5.7	-0.17	-1.98	3.16	1.56	0.024	
error	± 0.08	± 2.1	± 0.3	± 0.8	± 1.0	± 10	± 1.3	± 12.1	± 1.1	± 0.07	± 0.03	± 0.13	± 0.04	± 0.004

In contrast to the previously proposed [25] spin state with zig-zag chains in the ab plane containing spins 2, 3, 6, and 7, our spin state can be better described as a collection of c -axis chains or connected bitetrahedra [15,34] containing spins $\{1, 2, 3, 4\}$ or $\{5, 6, 7, 8\}$ and sketched in Fig. 1(c). These chains are weakly coupled within the ab plane by exchange couplings J_9 , J_{10} , and J_{12} . At zero field, the predicted spin state has angles $\phi_1 = -0.83\pi$, $\phi_2 = 0.40\pi$, $\phi_3 = -0.22\pi$, and $\phi_4 = 0.64\pi$.

What explains the wide range of J_i values? An orthorhombic distortion [25] with $b/(a\sqrt{3}) - 1 \rightarrow 0.018$ as $T \rightarrow 0$ breaks the hexagonal symmetry of the ab plane and explains the difference between the pairs $\{J_1, J_2\}$, $\{J_8, J_{11}\}$, and $\{J_{10}, J_{12}\}$. The difference between couplings like $\{J_7, J_8\}$ is caused by charge ordering: whereas J_7 couples moments 2 and 3 with $M_2 = M_3$, J_8 couples moments 2 and 4 with $M_2 \neq M_4$. Charge ordering also explains the difference between the pairs $\{J_2, J_3\}$ and $\{J_9, J_{10}\}$. Although not necessarily identical, J_{11} and J_{12} are assumed to be equal [35] because the spin state and excitations only depend on their average.

Our results indicate that the exchange coupling J_8 between moments 2 (Co^{2+}) and 4 ($\text{Co}^{3+}/\text{Co}^{2+}\underline{L}$) is strongly ferromagnetic. Larger in magnitude even than the 155 meV antiferromagnetic coupling found in the cuprate Nd_2CuO_4 [36], $J_8 \approx 183$ meV may be the largest exchange coupling ever reported. The strength of this coupling might be explained by the double-exchange mediated hopping of ligand holes \underline{L} [18] from site 4 to 2.

All the largest exchange couplings $J_1 = J_5 \approx -95$ meV, $J_3 = J_6 \approx 44$ meV, and $J_8 \approx 183$ meV lie within connected bitetrahedral, c -axis chains. Inside each chain, spins 2 and 4 are ferromagnetically coupled by J_8 , spins 1 and 2 are antiferromagnetically coupled by J_1 , and spins 4 and 1 are ferromagnetically coupled by J_3 . The competing exchange interactions among the trio of spins $\{1, 2, 4\}$ produces a non-collinear spin state within each chain.

The interaction between chains in the ab plane is dominated by the ferromagnetic $J_{10} \approx 30$ meV, which is still weaker than the interactions J_1 , J_3 , J_5 , J_6 and J_8 within each chain. Chain moments $M_{\text{ch}} = 1.34 \mu_B/\text{f.u.}$ are then ferromagnetically aligned along \mathbf{b} . Above $T_c = 70$ K, the short-range ferrimagnetic order within each chain may be responsible for the large, negative Curie-Weiss temperature $\Theta_{\text{CW}} \approx -1720$ [23] or -890 K [29], the larger than expected Curie constant [23], and the susceptibility anomaly [29] at 360 K suggestive of short-range magnetic order far above T_c .

Comparison between the theoretical and experimental results for the magnetization in Fig. 1(d) suggests that

roughly 20% of the sample is in domain I. Different domain populations in different samples may explain the discrepancies between the reported magnetization measurements [23,25,29–31].

Easy-axis anisotropies A and C favor ferrimagnetic alignment along \mathbf{b} rather than \mathbf{a} . The spin-flop (SF) field required to flip the spins towards the \mathbf{a} direction must increase as the field along \mathbf{b} increases [37]. As shown in the inset to Fig. 3(a), $B_{\text{SF}}(\psi)$ then increases with ψ . If $B_{\text{SF}}(\psi = 0) < 15$ T, then the MR spectrum for 15 T would show a discontinuity at the transition from a low-field (LF) to a high-field (HF) state below some critical value of ψ . Since the MR mode frequencies in Fig. 3(a) do not exhibit a discontinuity as a function of ψ , we conclude that $B_{\text{SF}}(\psi = 0)$ exceeds 15 T and probably, based on the smooth dependence of the magnetizations on field, exceeds 32 T as well. The apparent small size of B_{SF} [21,38] must reflect the net magnetization of all three domains. With $p_1 = 0.19$ and $p_2 + p_3 = 0.81$, the net magnetizations along $[1, 0, 0]$ and $[0, 1, 0]$ plotted in Fig. 1(d) are quite close. They become equal when $p_1 = 0.27$.

Given other conditions, our fit chooses the spin state that matches the powder-diffraction data [25] as closely as possible [39]. Spins \mathbf{S}_i are provided different magnetic form factors $F_i(Q) = 1/(1 + (Q/Q_i)^2)$. The scales $Q_i/4\pi$ are different for the three Co valences: $Q_1/4\pi = 0.052 \text{ \AA}^{-1}$, $Q_2/4\pi = Q_3/4\pi = 0.212 \text{ \AA}^{-1}$, and $Q_4/4\pi = 0.105 \text{ \AA}^{-1}$. Hence, Q_i decreases with increasing number of holes and Co moment size. All are smaller than the scale $Q_0/4\pi \approx 0.3 \text{ \AA}^{-1}$ measured by Khan and Erickson [40] for Co^{2+} in CoO .

Predicted modes below 5 THz are plotted in Fig. 2. The Goldstone modes for all three domains are lifted by in-plane anisotropies to become the MR modes with zero-field frequencies of 1.07 THz. As remarked earlier, the lower MR mode comes from domains II and III while the upper MR mode comes from domain I. Below 3.5 THz, one EM mode is produced in domain I and another in domains II and III. The EM mode from domain I must dominate the optical absorption. The predicted field dependence of the upper MR mode is quite close to the observed dependence. But the predicted curvature of the lower MR mode is not observed and the predicted slope of the EM mode has the wrong sign. These fits can be further improved by including next-neighbor exchange interactions.

The spin-induced polarization in $\text{CaBaCo}_4\text{O}_7$ is generated by the dependence of the exchange interactions J_{ij} on an electric field, called magnetostriction. Coupling constant λ_{ij} for bond $\{i, j\}$ is associated with the

spin-induced polarization [41] per site of $P_c^{ij} = \lambda_{ij} \mathbf{S}_i \cdot \mathbf{S}_j / 4$ (accounting for the four equivalent bonds per unit cell) with $\lambda_{ij} = \partial J_{ij} / \partial E_c$. The MR matrix element $\langle n | M_a | 0 \rangle$ mixes with the EM matrix element $\langle n | P_c^{ij} | 0 \rangle$ for domains II and III but not for domain I. Therefore, our model can explain the strong asymmetry [42] $\sim \text{Re}\{\langle n | \mathbf{M} \cdot \mathbf{B}_\omega | 0 \rangle \langle 0 | \mathbf{P} \cdot \mathbf{E}_\omega | n \rangle\}$ in the absorption of counter-propagating light waves [32] for the lower observed MR mode in geometry *ii* with $\mathbf{E}_\omega \parallel \mathbf{c}$. But it cannot explain the observed asymmetry of this mode in geometry *i* with $\mathbf{E}_\omega \perp \mathbf{c}$ if only $\langle 0 | P_c | n \rangle$ is significant.

We can enumerate the possible bonds responsible for the spin-induced polarization based on the observation that the EM mode has an absorption about 7.5 times that of the MR mode in zero field, rising to about 35 times the upper MR mode at 10 T. At both 0 and 10 T, the only bonds that generate spin-induced polarizations of the right magnitude are {1, 3}, {1, 4}, and {2, 3}, all within the *c*-axis chains.

From the relative absorptions at 10 T, we estimate that $\langle P_c \rangle \approx 720 \text{ nC/cm}^2$ for bond {1, 3}, 510 nC/cm^2 for bond {1, 4}, and 790 nC/cm^2 for bond {2, 3}, each with a different value for λ_{ij} . These results are consistent with the density-functional theory result [24] $\langle P_c \rangle \approx 460 \text{ nC/cm}^2$ but still smaller than the recently observed [21] polarization of 1700 nC/cm^2 . However, other measurements indicate that $\langle P_c \rangle$ ranges from 320 nC/cm^2 [30] to 900

nC/cm^2 [43]. Of course, more than one set of bonds may be responsible for the spin-induced polarization.

Our work has shown how ferrimagnetism and ferroelectricity coexist in an important multiferroic material. We have presented a nearly complete solution for the magnetization, spin state, and mode frequencies of $\text{CaBaCo}_4\text{O}_7$. An orthorhombic structural distortion above T_c partially relieves the geometric frustration on the kagome and triangular layers. Although the *c*-axis chains are ferromagnetically aligned on a triangular lattice, competing interactions within each chain produce a non-collinear spin state. Sets of bonds within each chain are responsible for the large spin-induced polarization of $\text{CaBaCo}_4\text{O}_7$. We are hopeful that high-field measurements can confirm the predicted SF transition above 32 T and that density-functional theory can explain the strongly ferromagnetic coupling J_8 .

Research sponsored by the U.S. Department of Energy, Office of Science, Basic Energy Sciences, Materials Sciences and Engineering Division (RF), by the Hungarian Research Funds OTKA K 108918, OTKA PD 111756, and Bolyai 00565/14/11 (SB, VK, and IK), and by the institutional research funding IUT23-3 of the Estonian Ministry of Education and Research and the European Regional Development Fund project TK134 (TR and UN).

¹ K. Binder and A.P. Young, *Rev. Mod. Phys.* **58**, 801 (1986).

² M.J. Harris, S.T. Bramwell, D.F. McMorrow, T. Zeiske, and K.W. Godfrey, *Phys. Rev. Lett.* **79**, 2554 (1997).

³ S. Mühlbayer, B. Binz, F. Jonietz, C. Pfleiderer, A. Rosch, A. Neubauer, R. Georgii, and P. Böni, *Science* **323**, 915 (2011).

⁴ D.I. Khomskii, *J. Magn. Magn. Mater.* **306**, 1 (2006).

⁵ S.-W. Cheong and M. Mostovoy, *Nat. Mat.* **6**, 13 (2007).

⁶ A.B. Sushkov, R.V. Aguilar, S. Park, S.-W. Cheong, and H.D. Drew, *Phys. Rev. Lett.* **98**, 027202 (2007).

⁷ Y. Yamasaki, S. Miyasaka, Y. Kaneko, J.-P. He, T. Arima, and Y. Tokura, *Phys. Rev. Lett.* **96**, 207204 (2006).

⁸ M. Soda, K. Kimura, T. Kimura, and K. Hirota, *Phys. Rev. B* **81**, 100406 (2010).

⁹ S. Seki, N. Kida, S. Kumakura, R. Shimano, and Y. Tokura, *Phys. Rev. Lett.* **105**, 097207 (2010).

¹⁰ K. Taniguchi, N. Abe, S. Ohtani, and T. Arima, *Phys. Rev. Lett.* **102**, 147201 (2009).

¹¹ F. Ye, R.S. Fishman, J.A. Fernandez-Baca, A.A. Podlesnyak, G. Ehlers, H.A. Mook, Y.-Q. Wang, B. Lorenz, and C.W. Chu, *Phys. Rev. B* **83**, 140401 (2011).

¹² M. Valdor and M. Andersson, *Sol. St. Sci.* **4**, 923 (2002); M. Valdor, *Sol. St. Sci.* **6**, 251 (2004).

¹³ E.V. Tsipis, D.D. Khalyavin, S.V. Shiryaev, K.S. Redkina, and P. Núñez, *Mat. Chem. Phys.* **92**, 33 (2005); E.V. Tsipis, V.V. Kharton, J.R. Frade, and P. Núñez, *J. Sol. St. Electrochem.* **9**, 547 (2005).

¹⁴ G.L. Bychkov, S.N. Barilo, S.V. Shiryaev, D.V. Sheptyakov, S.N. Ustinovich, A. Podlesnyak, M. Baran, R. Szymczak, and A. Furrer, *J. Cryst. Growth* **275**, e813 (2005).

¹⁵ L.C. Chapon, P.G. Radaelli, H. Zheng, and J.F. Mitchell, *Phys. Rev. B* **74**, 172401 (2006).

¹⁶ D.D. Khalyavin, P. Manuel, B. Ouladdiaf, A. Huq, P.W. Stephens, H. Zheng, J.F. Mitchell, and L.C. Chapon, *Phys. Rev. B* **83**, 094412 (2011).

¹⁷ A.K. Bera, S.M. Yusuf, and S. Banerjee, *Sol. St. Sci.* **16**, 57 (2013).

¹⁸ A. Maignan, V. Caaignaert, D. Pelloquin, S. Hébert, V. Pralong, J. Hejtmánek, and D. Khomskii, *Phys. Rev. B* **74**, 165110 (2006).

¹⁹ S. Avci, O. Chmaissem, H. Zheng, A. Huq, P. Manuel, and J.F. Mitchell, *Chem. Mat.* **25**, 4188 (2013).

²⁰ A. Huq, J.F. Mitchell, H. Zheng, L.C. Chapon, P.G. Radaelli, K.S. Knight, and P.W. Stephens, *J. Sol. St. Chem.* **179**, 1136 (2006).

²¹ V. Caaignaert, A. Maignan, K. Singh, Ch. Simon, V. Pralong, B. Raveau, J.F. Mitchell, H. Zheng, A. Huq, and L.C. Chapon, *Phys. Rev. B* **88**, 174403 (2013).

²² J.-H. Lee and R.S. Fishman, *Phys. Rev. Lett.* **115**, 207203 (2015).

²³ V. Caaignaert, V. Pralong, A. Maignan, and B. Raveau, *Sol. St. Comm.* **149**, 453 (2009).

²⁴ R.D. Johnson, K. Cao, F. Giustino, and P.G. Radaelli, *Phys. Rev. B* **90**, 045192 (2014).

²⁵ V. Caaignaert, V. Pralong, V. Hardy, C. Ritter, and B. Raveau, *Phys. Rev. B* **81** 094417 (2010).

²⁶ S. Chatterjee and T. Saha-Dasgupta, *Phys. Rev. B* **84**, 085116 (2011).

²⁷ R.S. Fishman, J.T. Haraldsen, N. Furukawa, and S. Miyahara, *Phys. Rev. B* **87**, 134416 (2013).

²⁸ Md. M. Seikh, V. Caignaert, V. Pralong, and B. Raveau, *J. Phys. Chem. Sol.* **75**, 79 (2014).

²⁹ Z. Qu, L. Ling, L. Zhang, and Y. Zhang, *Sol. St. Comm.* **151**, 917 (2011).

³⁰ H. Iwamoto, M. Ehara, M. Akaki, and H. Kuwahara, *J. Phys.: Conf. Ser.* **400**, 032031 (2012).

³¹ Md. M. Seikh, T. Sarkar, V. Pralong, V. Caignaert, and B. Raveau, *Phys. Rev. B* **86**, 184403 (2012).

³² S. Bordács, V. Kocsis, Y. Tokunaga, U. Nagel, T. Rőm, Y. Takahashi, Y. Taguchi, and Y. Tokura, *Phys. Rev. B* **92**, 214441 (2015).

³³ The THz spectra of CaBaCo₄O₇ were measured with linear light polarization using Fourier-transform spectroscopy [32]. The reference spectrum was taken in zero field.

³⁴ M. Valdor, *J. Phys.: Cond. Mat.* **16**, 9209 (2004).

³⁵ Since J_{11} and J_{12} are intra- and inter-chain couplings, respectively, they contribute differently to the critical temperature.

³⁶ P. Bourges, H. Casalta, A.S. Ivanov, and D. Petitgrand, *Phys. Rev. Lett.* **79**, 4906 (1997).

³⁷ While the coplanar LF spin state has a lower energy than the HF state below 32 T, it becomes locally unstable to a buckled state with spins canted out of the *ab* plane between 16 and 32 T for field along **a**. Based on the smooth depen-

dence of the magnetizations on field, the transition from the coplanar to the buckled state must be second order.

³⁸ V. Pralong, V. Caignert, T. Sarkar, O.I. Lebedev, V. Dufort, and B. Raveau, *J. Sol. St. Chem.* **184**, 2588 (2011).

³⁹ Fitting only the powder data [25], our spin state gives $\chi^2 = 0.046$ compared to $\chi^2 = 0.021$ for the spin state ($\phi_1 = -0.24\pi$, $\phi_2 = \phi_3 = 0.67\pi$, and $\phi_4 = -0.44\pi$) based solely on that data.

⁴⁰ D.C. Khan and R.A. Erickson, *Phys. Rev. B* **1**, 2243 (1970).

⁴¹ Based on the symmetry of adjacent layers, it is easy to show that the polarization operator \mathbf{P}^{12} associated with bond {1, 2} has components

$$P_a^{12} \propto C_{12} - C_{56} - C_{1'2'} + C_{5'6'},$$

$$P_b^{12} \propto C_{12} + C_{56} - C_{1'2'} - C_{5'6'},$$

$$P_c^{12} \propto C_{12} + C_{56} + C_{1'2'} + C_{5'6'},$$

where $C_{ij} = \mathbf{S}_i \cdot \mathbf{S}_j$. Similar relations hold for other bonds. Only the *c* component P_c^{ij} can produce a static polarization but all three components may contribute to the off-diagonal polarization matrix elements $\langle 0 | P_\alpha^{ij} | n \rangle$ ($n \neq 0$).

⁴² S. Miyahara and N. Furukawa, *J. Phys. Soc. Japan* **80**, 073708 (2011).

⁴³ V. Kocsis, S. Bordács, and I. Kézsmárki, (unpublished).